Applied Surface Science 623 (2023) 157001

Contents lists available at ScienceDirect

Applied Surface Science

journal homepage: www.elsevier.com/locate/apsusc

Full Length Article

Understanding the potential-induced activation of a cobalt MOF electrocatalyst for the oxygen evolution reaction

Silvia Gutiérrez-Tarriño [a], Arismendy Portorreal-Bottier [b], Susana Trasobares [c,d], Juan José Calvente [b], Jose J. Calvino [c,d], José Luis Olloqui-Sariego [b,*], Pascual Oña-Burgos [a,e,*]

[a] Instituto de Tecnología Química, Universitat Politècnica de València-Consejo Superior de Investigaciones Científicas (UPV-CSIC), Avda. de los Naranjos s/n, 46022 Valencia, Spain
[b] Departamento de Química Física, Universidad de Sevilla, Profesor García González 1, 41012 Sevilla. Spain
[c] Departamento de Ciencia de los Materiales e Ingeniería Metalúrgica y Química Inorgánica, Facultad de Ciencias, Universidad de Cádiz, Campus Río San Pedro S/N, Puerto Real 11510, Cádiz, Spain
[d] Instituto Universitario de Investigación de Microscopía Electrónica y Materiales (IMEYMAT), Facultad de Ciencias, Universidad de Cádiz, Campus Río San Pedro S/N, Puerto Real 11510, Cádiz, Spain
[e] Departamento de Química y Física, Centro de Investigación CIAIMBITAL, Universidad de Almería, Ctra. Sacramento, s/n, 04120 Almería, Spain

ARTICLE INFO

Keywords:
MOF-electrode interface
Electrochemical activation
Structural evolution
Advance microscopy techniques
Electrocatalytic oxygen evolution reaction
2D-Cobalt-MOF

ABSTRACT

Metal–organic frameworks (MOFs) are attractive porous materials for electrocatalytic applications associated with carbon-free energy storage and conversion. This type of material usually requires a post-treatment to be used as electrocatalyst. The present work comprehensively investigates the electrochemical activation of a cobalt-MOF@Nafion composite that produces outstanding electrocatalytic performance for the water oxidation reaction at neutral pH. A detailed electrochemical characterization reveals that the electroactivation of the composite requires the participation of the oxygen evolution reaction (OER) and leads to a significant increase in the electroactive population of cobalt centers. It is shown that an increase of the applied activation potential in the OER region results in a faster electroactivation of the Co-MOF without affecting the intrinsic electrocatalytic properties of the active cobalt centers, as evidenced by the unique linear correlation between the electrocatalytic OER current and the population of electroactive cobalt. In addition, at structural level, it is shown that the electrochemical activation causes the partial disruption of the Nafion adlayer, as well as morphological changes of the Co–MOF particles from a compact, rounded morphology, before electrochemical activation, to a more open and expanded structure, after electroactivation; with the concomitant increase of the number of surface–exposed cobalt centers. Interestingly, these cobalt centers retain their coordinative chemistry and their laminar distribution in the nanosheets at the nanoscale, which is consistent with the preservation of their intrinsic electrocatalytic activity after potential–induced activation. In this scenario, these results suggest that only the electroactivated cobalt centers with good accessibility to the electrolyte are electrochemically active. This work provides a better understanding of the processes and structural changes underlying the electrochemical activation at neutral pH of a Co–MOF for boosting the electrocatalytic water oxidation reaction.

1. Introduction

Water electrolysis has been widely considered to be a feasible and clean process related with energy storage and conversion.[1–3] The overall water splitting process includes both hydrogen evolution reaction (HER) and oxygen evolution reaction (OER), among which the OER is an uphill energy transformation process involving four-proton and four-electron transfers per oxygen molecule.[4] Therefore, many efforts in the electrochemistry and material science fields are focused on the development of efficient electrocatalysts for the thermodynamically and kinetically impaired OER reaction.[5].

Metal–Organic Frameworks (MOFs) are emerging as novel porous materials with appealing characteristics to be applied as electrocatalysts, due to their large surface area, highly ordered structure, large

* Corresponding authors at: Instituto de Tecnología Química, Universitat Politècnica de València-Consejo Superior de Investigaciones Científicas (UPV-CSIC), 46022 Valencia, Spain; Departamento de Química y Física, Centro de Investigación CIAIMBITAL, Universidad de Almería, 04120, Spain (P. Oña-Burgos).
E-mail addresses: jlolloqui@us.es (J.L. Olloqui-Sariego), pasoabur@upvnet.upv.es (P. Oña-Burgos).

https://doi.org/10.1016/j.apsusc.2023.157001
Received 15 December 2022; Received in revised form 11 February 2023; Accepted 10 March 2023
Available online 13 March 2023

porosity, controllable arrangement of isolated active sites and high design flexibility.[6–9] However, this type of materials has typically suffered from low conductivity and low electrocatalytic activity.[10] Strategies reported to overcome these limitations have focused on the improvement of charge transport across the MOF and the modulation of their electronic environment via pre– or post– synthetic methods. For instance, by tuning the synthetic protocol, the electronic conductivity of MOFs has been improved by introducing donor–acceptor type interactions,[11–13] mixed valent states of the node/linker,[14,15] and π-π stacking or π-conjugation into the framework. Furthermore, incorporation of missing linker and missing node defects[16–20] have been shown to enhance the catalytic activity of MOFs by modulating the electronic structures of their building units. Besides, other strategies have focused on the increase of the accessibility to the active sites by designing hybrid MOF heterostructures containing two or more different kinds of metal ions or organic linkers.[21–23] On the other hand, post synthetic approaches are mostly intended to optimize coordinative unsaturated metal sites of MOFs and include solvent assisted ligand exchange,[17] plasma engraving[24,25] or electrochemical activation.[26–28].

Nevertheless, most of the reported MOFs are poorly stable both in chemical and electrochemical environments because of the complexity of MOFs structures and their possible conversion paths during electrocatalysis, thereby acting as mere precatalysts for electrocatalytic applications.[29] Indeed, most of the reported MOF electrocatalysts for OER operate more effectively in strongly alkaline media, where they are typically unstable. Under these conditions, organic fragments of the MOFs decompose and mostly convert into an open framework oxide-based structure.[26,30] In this context, several works have recently monitored the electrochemical activation of MOF–modified electrodes under strongly alkaline conditions and reported a phase transformation into oxy(hydroxide) species, with concomitant loss of the structural integrity of the MOF framework.[31–36] This common, and often overlooked, structural reconstruction of MOFs within alkaline media should be carefully considered when stablishing the feasibility and efficiency of these materials as real OER electrocatalysts. On the other hand, under electrochemical conditions with a voltage bias applied, the MOF reconstruction in alkaline media has been also ascribed to changes in the local pH at the interface, to redox reactions involving extensive chemical bond breaking/formation on the metal sites, and to linker degradation by radical intermediates during electrocatalysis.[27,37–41] Only few works have reported on stable MOFs where the material is likely to be stable and robust, but most of them require an electrochemical activation to boost the OER.[4,17,42,43] However, this activation process has been poorly addressed, so it is not well understood yet. Thus, understanding this phenomenon is key to rationalize it and to establish structure–activity relationships. In a recent work,[43] we reported that the electrochemical activation of the composite formed by a cobalt MOF and Nafion promotes the formation of the electrocatalytically active cobalt species for an efficient oxygen evolution reaction. This activation process parallels the enhancement of the charge transport across the MOF film. However, the origin of the electrochemical activation is unknown and the possible structural and morphological changes on the bulk MOF accompanying the activation process is unclear.

To get more insights into the factors underlying the electrochemical activation, here we have studied the effect of the applied potential on the electroactivity of a double nanosheet cobalt MOF (**2D-CoMOF**) combined with a deep structural characterization by using a variety of complementary techniques, including X-ray diffraction (XRD), Raman spectroscopy, high resolution high-angle annular dark field-scanning transmission electron microscopy (HAADF-STEM), energy-dispersive X-Ray spectroscopy-scanning transmission electron microscopy (STEM-XEDS) and electron energy loss spectroscopy (EELS). In this context, microscopy techniques are valuable to probe the structural evolution of the MOF at microscopic scale during the potential induced activation. However, the high electron beam-sensitivity of the MOFs limits their use. In this work, this limitation has been overcome by using the innovative integrated Differential Phase Contrast scanning transmission electron microscopy technique (iDPC–STEM), that allows recording structural images at very low electron dose and low voltages. Additionally, when used in aberration corrected microscopes, this technique allows obtaining novel high-resolution images of activated MOF composite.

Herein, we show for the first time that the electrochemical activation of a composite of **2D-MOF@Nafion** at neutral pH is boosted by the oxygen evolution reaction (OER) and results in a significant increase in the number of electroactive sites, with the concomitant enhancement of the catalytic current intensity. The linear correlation between the catalytic current and the number of the generated electroactive cobalt centers reveals that the electrochemical activation does not affect the intrinsic electrocatalytic activity of the material, but only the number of the electrochemically active sites. It is also shown that an increase of the activation potential into OER region accelerates the activation process, without affecting this abovementioned linear correlation. In addition, the structural characterization showed that the electrochemical activation leads to morphological changes of the composite caused by the dissemination of the Nafion adlayer and the concomitant decompaction of the **2D-MOF@Nafion** particle aggregates, resulting in an increase of the active metal centers exposed to the surface. More interestingly, and in contrast with the typically reported phase transition in the alkaline electroactivation of MOF, it is also demonstrated that both the coordinate bonding between metal nodes and organic linker and the crystallinity are preserved at nanoscale. This finding matches with the preservation of the intrinsic electroactivity of this material during their potential–induced activation.

2. Results and discussion

2.1. Potential induced activation

First, the pristine **2D-CoMOF** was dispersed onto an alcoholic solution of Nafion. The influence of Nafion on the morphology and electronic structure of the initial π-stacked **2D-CoMOF** has been studied by means of FESEM, PXRD, Raman spectroscopy and XPS (Fig. S1). Then, the resulting composite **2D-CoMOF@Nafion** was deposited onto a graphite electrode to study the effect of the applied potential on its electrochemical activation. The voltammetric response of the **2D-CoMOF@Nafion**-modified electrode was measured in an aqueous 0.1 M sodium phosphate buffer solution at pH 7 and 25 °C. As seen in Fig. 1a, the voltammetric response consists of a poorly defined voltammetric wave, located at 0.80 V (vs. Ag/AgCl/NaCl sat.), which corresponds to the Co(II)/Co(III) redox conversion, superimposed to a subtle rising background current, which is ascribed to the electrocatalytic oxidation of water. Contrary to what is expected, this result indicates that the MOF composite is almost electrochemically “silent”, and the population of electrocatalytically active sites is low. However, it was found that cycling the electrode with 1000 potential scans within the 0.1–1.1 V potential window, both the incipient voltammetric wave and the electrocatalytic branch progressively increased (Fig. S2), delineating a potential-induced process that promotes the generation of electroactive cobalt sites that boost the electrocatalytic water oxidation.

For a better control and follow-up of the activation process, a sequence of activation potential pulses (at 0.95 V for 10 min) with intermediate voltammetric interrogation was applied (inset in Fig. 1b–c). Voltammograms were measured by using both a stationary electrode (Fig. 1b) and a rotating disk electrode (RDE, Fig. 1c), the latter being used to quantify the OER electrocatalytic current under steady-state conditions for mass transport. As shown in Fig. 1b–c, an increase in the number of activation pulses results in an increase of both the Co(II)/Co(III) voltammetric wave and the electrocatalytic current associated with the OER, both findings being consistent with an increase in the

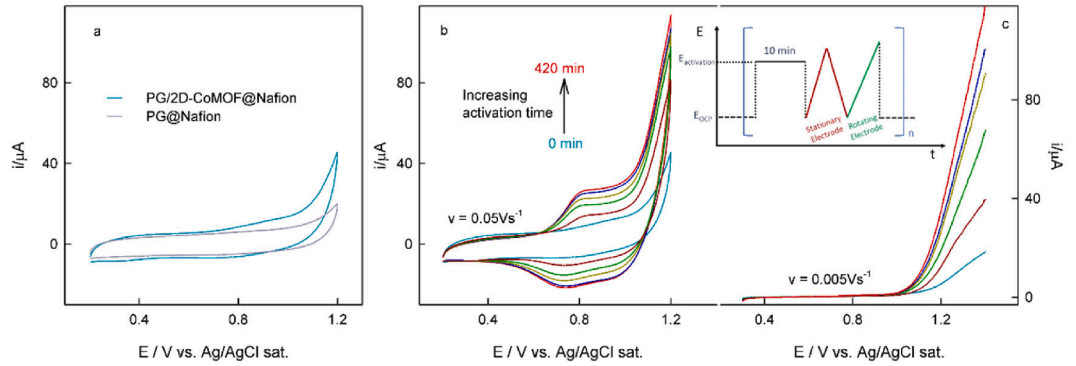

Fig. 1. (a) Cyclic voltammograms recorded at 0.05 Vs^{-1} of a pyrolytic graphite electrode modified with Nafion (grey dashed line) or with non–activated **2D-CoMOF@Nafion** (Cyan line); (b) Cyclic voltammograms recorded at 0.02 Vs^{-1} of **2D-CoMOF@Nafion** at different times during electrochemical activation at 0.95 V. Inset plot: Illustration of the pulse method used for monitoring the electrochemical activation. (c) Their corresponding rotating disk voltammograms for OER recorded at 5 mVs^{-1} and 1500 rpm. Other experimental conditions: 0.1 M SPB solution pH 7 at 25 °C. (For interpretation of the references to colour in this figure legend, the reader is referred to the web version of this article.)

electroactive population of cobalt centers. The surface concentration of electroactive cobalt Γ can be determined from $\Gamma = Q/(nFA)$, where Q is the faradaic charge under the baseline-corrected voltammetric wave preceding the electrocatalytic branch, n is the number of electrons transferred per cobalt center, A is the geometric surface area of the graphite electrode, and F is the Faraday constant. Fig. 2a shows how Γ increases non-linearly with the activation time, following the typical logarithmic growth pattern that ends in a limiting plateau value for sufficiently long times.

To probe whether the increase of the electrocatalytic current during the potentiostatic activation of the MOF is merely due to an increase of the electroactive population of cobalt centers or to an additional improvement of their intrinsic electrocatalytic properties, we have plotted in Fig. 2b (red symbols) the electrocatalytic current at a fixed potential of 1.15 V against surface concentration of electroactive cobalt. The observed linear correlation reveals that the enhancement of the electrocatalytic current is solely due to the increase of the number of electroactive cobalt centers, since otherwise a non–linear dependence is expected.

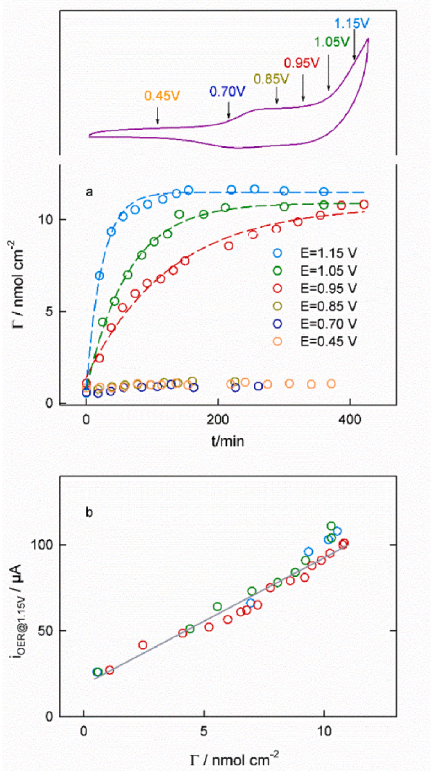

Fig. 2. (a) Variation of the electroactive cobalt surface concentration along electrochemical activation at the indicated applied potentials, and (b) the corresponding variation of the electrocatalytic current at a fixed potential (1.15 V) with the amount of cobalt centers of a pyrolytic graphite electrode modified with **2D-CoMOF@Nafion**. Other experimental conditions: 0.1 M SPB solution pH 7 at 25 °C.

In order to further explore whether the electrochemical activation requires the OER to take place, we studied the effect of varying the applied potential along the whole voltammogram, in such a way that the selected activation potentials cover both the non-faradaic and faradaic regions of the voltammetric scan (Fig. 2a). As can be observed, the electrochemical activation does not operate for applied potentials below 0.95 V, even at potentials where the Co(II)/Co(III) redox conversion proceeds (i. e. 0.7 and 0.85 V), whereas, for activation potentials in the OER region (≥0.95 V), the rate at which the electroactive population grows increases with the applied potential, as evidenced by the steeper variation of Γ with the activation time. This result clearly indicates that the electroactivation of the composite is boosted by the oxygen evolution reaction (OER), so that it may involve the presence of some of the reactive oxygen species as well as oxygen bubbles. Moreover, the independence of the limiting plateau value of Γ with the applied potential corroborates that it corresponds to the maximum electroactive population of a completely activated electrode.

Interestingly, it was found that the activation potential does not affect the correlation of the electrocatalytic OER current (at 1.15 V) with the electroactive population of cobalt centers (Fig. 2b), as all i_{OER} vs. Γ data obtained for the different applied activation potentials follow the same linear trend. This finding corroborates that the potential-induced enhancement of the electrocatalytic current is solely due to an increase of the electroactive population of cobalt centers, without affecting their intrinsic electrocatalytic performance. Accordingly, the most plausible scenario involves a structural rearrangement of the composite during the activation process triggered by the OER that improves the accessibility of the electrolyte to the cobalt centers without significantly affecting their coordination chemistry. To assess the role of the Nafion on the electroactivation process, we performed electroactivation experiments with different Nafion contents in the composite. As can be seen in Fig. S3, a decrease of the Nafion content results in a faster electroactivation, without significantly affecting the correlation between the electrocatalytic OER current and the electroactive population of cobalt centers. This indicates that the final phase of the composite does not depend on the Nafion content, but rather exerts a blocking effect. Moreover, the insensitivity of the initial amount of electroactive cobalt centers to the Nafion content suggests that the

increase of the electroactive population during electroactivation requires structural rearrangement of the Co-MOF particles.

In addition, the stability of the activated MOF composite was explored by performing a chronoamperometric experiment comprising a first electrochemical activation step of the Co–MOF–modified electrode, and a subsequent long–term water electrolysis, both at 1.15 V and pH 7 (Fig. S4). The latter is characterized by a constant current during the 10 h of operation, which reveals the high stability of this material. In fact, the similarity of the cyclic voltammograms measured for the fully activated **2D-Co-MOF**, before and after the water electrolysis experiment, is consistent with the preservation of the electroactive cobalt population.

2.2. Probing coordinative changes

To probe whether the electrochemical activation of the MOF involves coordinative and/or structural and morphological changes, an in–depth characterization with spectroscopic and microscopy techniques was performed. As shown in a previous work,[43] the pristine **2D-CoMOF** is composed of double nanosheets held together by π–π interactions between the axial pyridine ligands. In contact with an aqueous solution, the pyridine ligands are displaced by water molecules leading to a more disordered material. To explore the effect of the electrochemical activation on the coordinative chemistry of the cobalt centers, we have measured the Raman and XPS spectra of the **2D–CoMOF@Nafion** composite before and after the application of the bias potential of 0.95 V. As shown in Fig. 3, no significant changes are observed in the Raman bands after electrochemical activation. More specifically, the bands associated with the organic linkers bipyridine (774, 1022 and 1278 cm^{-1}) and the carboxylic groups (1289, 1426, 1546 and 1615 cm^{-1}) remain unchanged, indicating that the electrochemical activation has a limited impact on the coordinative chemistry of the cobalt centers.

To further prove the absence of coordination changes during the electrochemical activation, we have also characterized the **2D–CoMOF@Nafion** composite by XPS spectra (Fig. 4). Although the binding energy value is typically used in XPS to determine the oxidation number of a chemical element, for the 3d transition elements, the spin–orbit splitting provides more information.[44] According to theoretical calculations,[45] the Co $2p_{1/2}$ − Co $2p_{3/2}$ spin − orbit splitting increases with the number of unpaired 3d, being close to 16 eV for high-spin Co(II) and to 15 eV for Co(III). For the current **2D–CoMOF@Nafion** composite before and after electrochemical activation the spectra show characteristic values of the high spin cobalt(II) compounds (Fig. 4a), [46–51] indicating that the cobalt centers of **2D-CoMOF** are mainly in the Co(II) oxidation state. In addition, the O 1 s peak, for the composite before and after electrochemical activation, was deconvoluted into four components (Fig. 4b), corresponding to Co-O (528.7 eV) of the water molecules coordinated to the cobalt center, O = C − O and C − O (531.5 and 532.9, respectively) associated to the carboxylate groups of the 2,2′-bipyridine-4,4′-dicarboxylic acid ligand, and FC-O-CF_2 (535.2 eV) ascribed to the Nafion wrapping. Interestingly, after electrochemical activation a decrease of the F_2C-O-CF_2 contribution can be observed, which is due to the partial loss of Nafion (*vide infra*). Finally, the N 1 s peak has only one contribution at 399.4 eV for both activated and non-activated MOF, characteristic of pyridinic nitrogen from the 2,2′-bipyridine-4,4′-dicarboxylic acid organic linkers (Fig. 4c). Overall, apart from the loss of the Nafion content on the surface, these results point out to a non-significant change of the surface structure of the MOF catalyst film during the electrochemical activation (More information in Table S1).

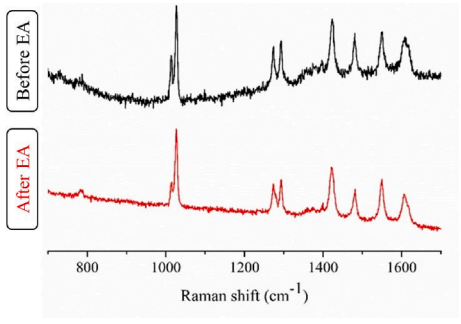

Fig. 3. Raman spectra of **2D-CoMOF@Nafion** composite before (black) and after (red) electrochemical activation at 0.95 V in a 0.1 M SPB solution pH 7 at 25 °C. (For interpretation of the references to colour in this figure legend, the reader is referred to the web version of this article.)

2.3. Probing structural changes

At the microscopic scale by FESEM (Field Emission Scanning Electron Microscopy), only small textural changes of the sample are observed (Fig. S5). Therefore, to get a more detailed view of the structural and morphological changes undergone by the **2D-CoMOF@Nafion** composite during its electrochemical activation, an advanced characterization at nanoscopic and atomic level was performed using the combination of HR HAADF-STEM and iDPC-STEM imaging techniques, with a current of around 0.5 pA (60 $e^{-}\cdot Å^{-2}$) to minimize sample damage. Fig. 5a and b show low and high magnification STEM-HAADF images, respectively, of the composite measured before its electrochemical activation. As seen in the images, the composite is comprised of aggregates of large, compact and rounded Co–MOF particles (200–370 nm). The smooth HAADF profile (Fig. 5c) reveals a low surface roughness, with the concomitant low population of surface–exposed cobalt centers with respect to the inner population in the particle core.

HAADF images at higher magnification with their corresponding elemental maps (Co, N, O, F) measured for an aggregate of three particles before electrochemical activation are depicted in Fig. 6. First, the spatial correlation of Co, O and N maps (Fig. 6c–e) highlights the coordination chemistry of the MOF. In addition, the superposition of the Co and F maps (Fig. 5f) reveals that the MOF particles are surrounded by a Nafion shell with a thickness of roughly 20–30 nm. The intensity profiles of the Co and F signals (Fig. 6g) evidence the uniformity of the Nafion adlayer and its accumulation in the interparticle space. On the other hand, comparison of XEDS spectra recorded at the core of the particle (location 1 in Fig. 6f) and at its shell (location 2 in Fig. 6f) reveals the absence of Co-leaching into the Nafion film during the preparation of the composite. Bearing in mind that this thick Nafion layer may partially block the access of the electrolyte component to the cobalt centers, it might contribute to the initial low electroactivity of the pristine MOF in the **2D-CoMOF@Nafion** composite. It should be noted that similar findings have been obtained from the STEM images obtained for other representative samples of the MOF composite (Fig. S5).

Electrochemical activation promotes significant textural changes in the **2D-CoMOF@Nafion** composite. As seen in the STEM-HAADF image at low magnification of an electrochemically treated composite (Fig. 5d), the original aggregates of rounded particles transform into an expanded and irregular composite, generating a more opened and porous structure. Indeed, high magnification STEM-HAADF images of dispersed particle aggregates activated potentiostatically (Fig. 5e), clearly show wrinkles and corrugation, as well as faint contrast spots in the aggregate that confer a sponge–like texture, with an increased microporosity. The HAADF intensity profile of this electrochemically activated composite (Fig. 5f) reveals a roughening of the surface, which is consistent with the formation of micropores in the MOF. Generated micropores of ≈ 15 nm are clearly distinguishable in the HAADF–STEM image and its corresponding intensity profile of a zoomed area of a MOF particle after electrochemical activation (Fig. S6). The protuberances resulting after electrochemical activation of the MOF composite increase the number of surface–exposed metal centers, which is crucial to promote their redox conversion.

To probe whether these structural changes induced by the potential

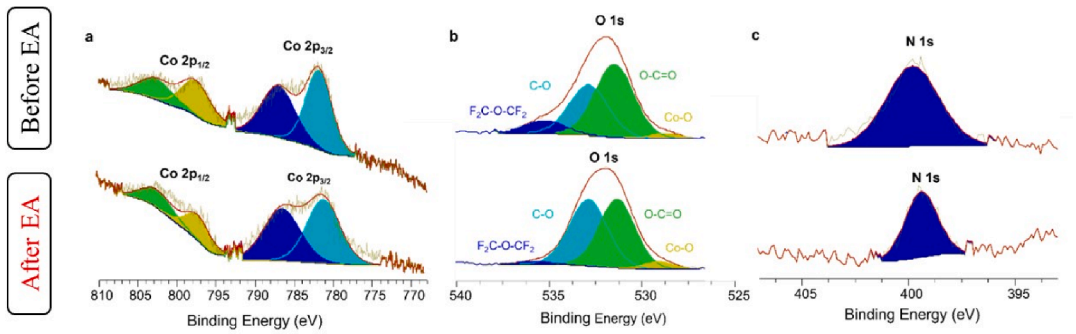

Fig. 4. XPS spectra of (a) Co 2p line, (b) O 1 s line and (c) N 1 s line of **2D-CoMOF@Nafion** before (above) and after (below) electrochemical activation at 0.95 V in a 0.1 M SPB solution pH 7 at 25 °C.

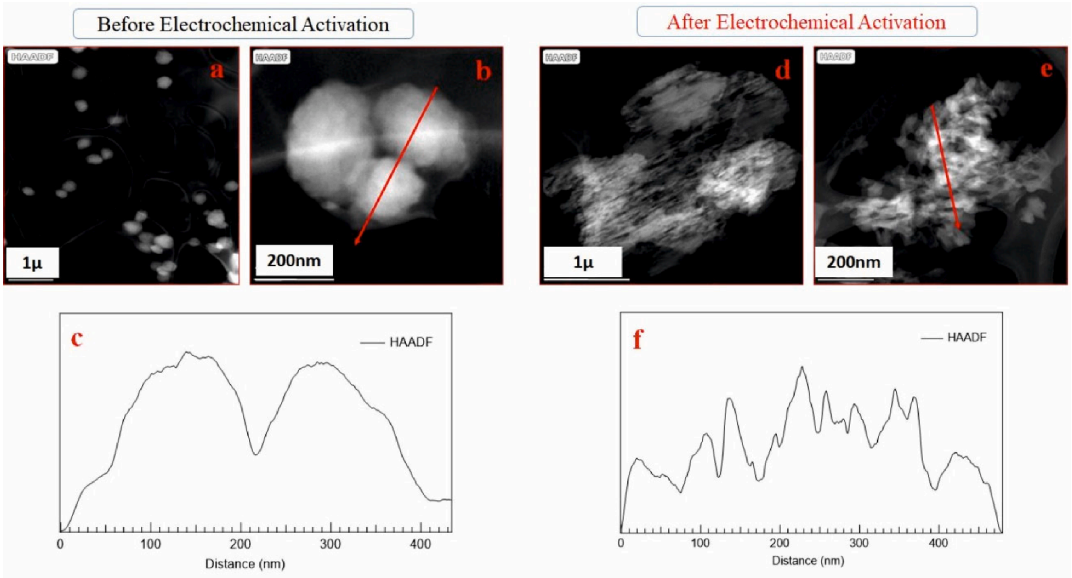

Fig. 5. STEM study of the **2D-CoMOF@Nafion** composite before (a-c) and after (d-f) electrochemical activation at 0.95 V in a 0.1 M SPB solution pH 7 at 25 °C. (a–b and d–e) STEM-HAADF images; (c) Line profiles of the HAADF along the path marked with a red arrow in (b); and (f) Line profiles of the HAADF along the path marked with a red arrow in (e). (For interpretation of the references to colour in this figure legend, the reader is referred to the web version of this article.)

are restricted to the MOF shell covering the MOF particles or they are also extended to the MOF matrix, the elemental maps for a typical aggregate of electrochemically activated MOF particles were imaged (Fig. 7). The elemental map of F (Fig. 7b) now reveals a spot–like distribution of fluorine which is consistent with a dissemination of the Nafion shell, probably due to its partial disruption. Superposition of the Co and F maps (Fig. 7f) and of their profile (Fig. 7g), together with the presence of the F and Co signals on the XEDS spectrum along the whole path (Fig. 7h) corroborates the significant loss of the initial Nafion shell.

On the other hand, the Co map (Fig. 7c) shows a more scattered distribution of the cobalt centers in the electrochemically treated sample than in its pristine state. This is supported by the extremely irregular pattern of the cobalt HAADF signal profile, which agrees with a significant increase of the cobalt centers accessible to the electrolyte, so that textural and morphological changes accompanying the electrochemical activation of the composite are not only present in the Nafion adlayer but also in the MOF particles. It should be noted that similar results were obtained from the images and analytical characterization of other representative MOF samples activated at a different potential of 1.1 V (Fig. S7), indicating that the structural rearrangement occurring during the electrochemical activation is independent on the applied potential for values higher than 0.95 V, where OER occurs. Overall, STEM results evidence that the electrochemical activation promotes much thinner and smaller particle size of **2D-CoMOF** aggregates, inducing the formation of micropores into the composite, which translates into a more expanded and accessible MOF, and thereby into a larger amount of electroactive cobalt centers. It has been demonstrated that this structural evolution improves the charge transport across the MOF, which strongly match with our previous results on the impedance measurements of the activated MOF,[43] and promotes the formation of active sites, thus enhancing the MOF catalytic activity.[52].

Interestingly, the perfect spatial correlation of Co, O and N maps of the composite after electrochemical activation of a MOF aggregate (Fig. 7c–e) clearly indicates that the MOF retains its coordinative chemistry, in agreement with the spectroscopic results. The preservation of the coordinate bonding between metal nodes and organic linkers is envisaged to be critical for their outstanding OER activity at neutral pH.

Finally, the crystallinity of the composite at the nanoscale after electrochemical activation was examined by means of integrated differential phase contrast (STEM-iDPC) imaging. Comparison of the STEM-iDPC image of a zoomed area (Fig. 8) of the electrochemically treated **2D-CoMOF@Nafion** composite and the pristine **2D-CoMOF**, reveals that the opened and rougher **2D-CoMOF@Nafion** structures generated during the electrochemical activation still retain the crystalline structure of the pristine **2D-CoMOF**. Concerning the starting material (Fig. 8a), the analysis in the spatial frequency space of images recorded on pristine **2D-CoMOF** crystallites reveal the presence of lattice spacings at 0.73 nm, 0.63 nm and 0.55 nm, close to those

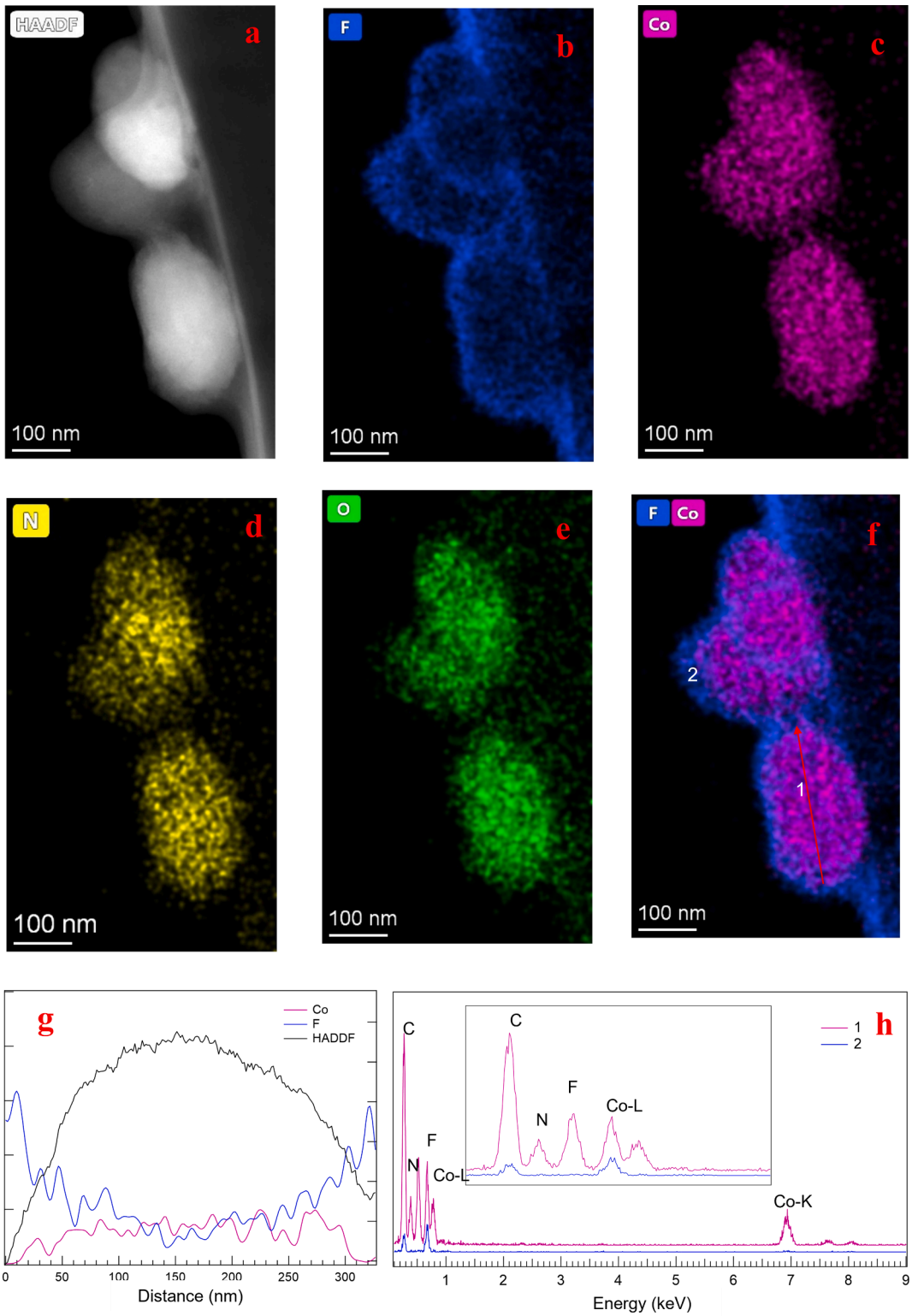

Fig. 6. STEM study at high magnification of the **2D-CoMOF@Nafion** composite before electrochemical activation. (a) STEM-HAADF image, (b-e) F, Co, N, and O, respectively, elemental maps, (f) overlayed Co-F maps, (g) Line profiles of the HAADF, F and Co signals along the path marked with a red arrow in (f). (g) XEDS spectra corresponding to the locations 1 and 2 marked in (f). (For interpretation of the references to colour in this figure legend, the reader is referred to the web version of this article.)

corresponding to the (−1 1 1), (10–2) and (11–2) planes of this phase (inset in Fig. 4a). Additional images are included in the Supported Information, where other lattice planes are also detected (Fig. S8). STEM-iDPC images of **2D-CoMOF@Nafion** after electrochemical activation, Fig. 8b, also reveal very large areas depicting lattice planes at roughly 0.82 nm, a distance slightly larger than that separating adjacent double nanosheets in the layered pristine **2D-CoMOF** structure (0.78 nm) ((1 1 0) planes). This enlargement could be very likely associated with the volume expansion during OER. Indeed, the elongated pores observed in the STEM-HAADF images run parallel to the direction of the double

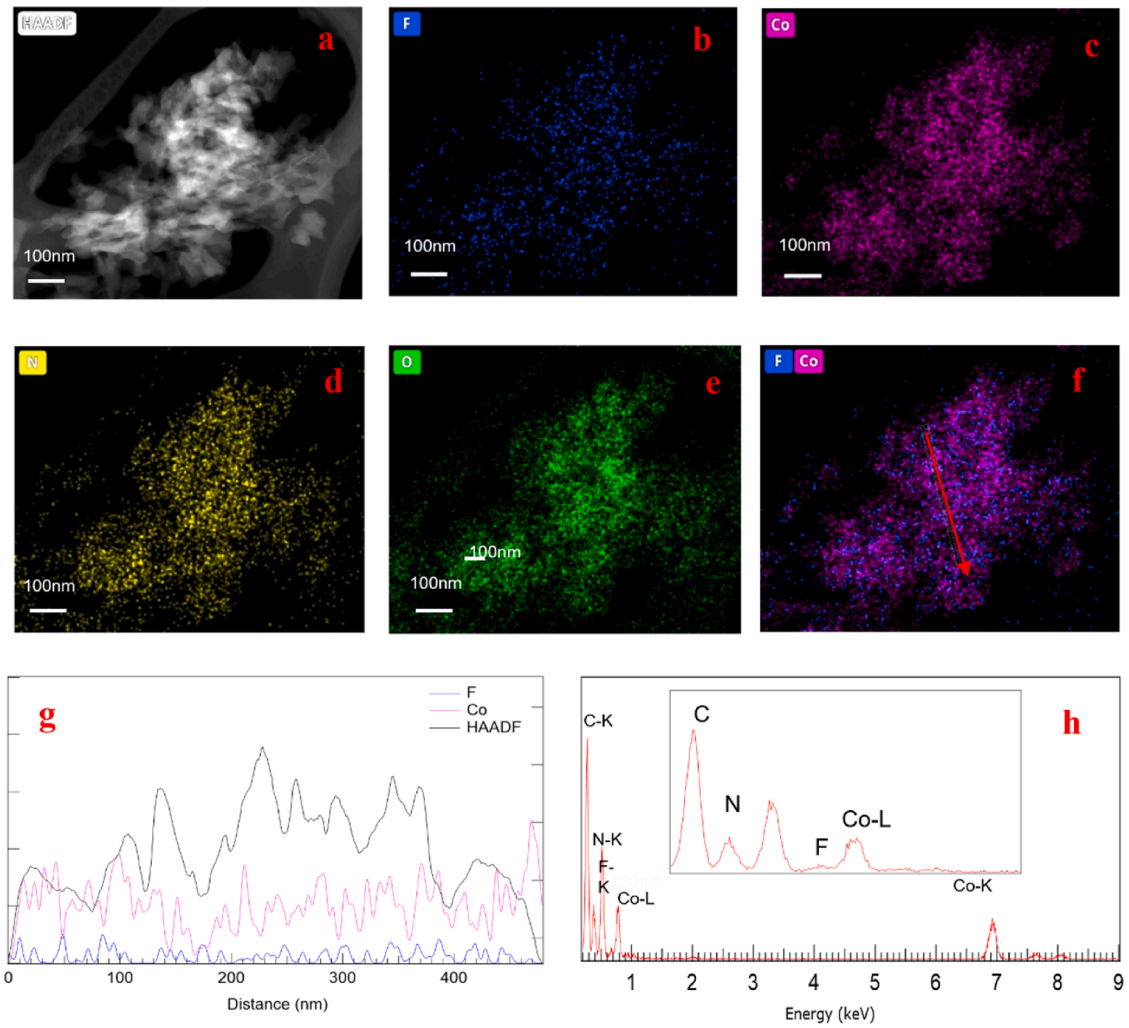

Fig. 7. STEM study at high mag of the **2D-CoMOF@Nafion** composite after electrochemical activation at 0.95 V in a 0.1 M SPB solution pH 7 at 25 °C. (a) STEM-HAADF image; (b-e) F, Co, N and O elemental maps, respectively; (f) Overlayed F-Co elemental maps. (g) Line profiles of the HAADF, F and Co signals along the path marked with a red arrow in (f). (g) XEDS spectra corresponding to the path marked with a red arrow in (f). (For interpretation of the references to colour in this figure legend, the reader is referred to the web version of this article.)

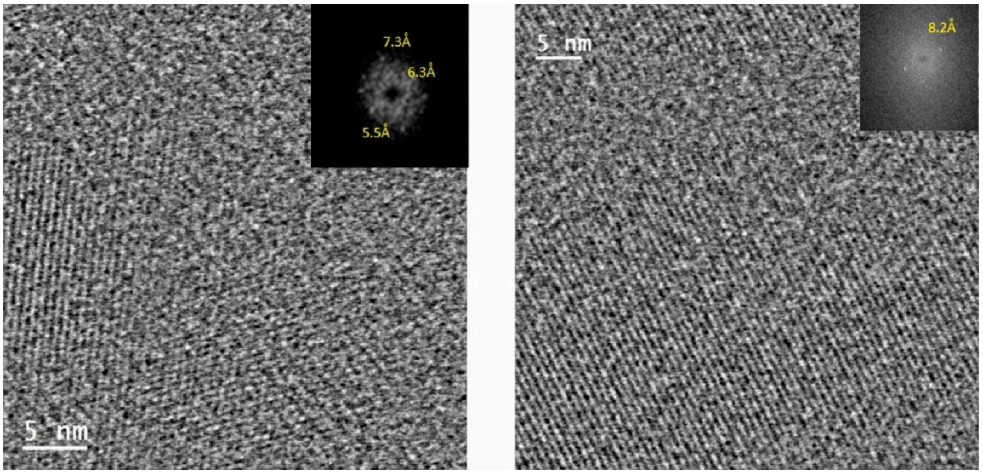

Fig. 8. High Resolution STEM-iDPC images recorded on (a) the starting **2D-CoMOF** material and (b) the **2D-CoMOF@Nafion** composite after electrochemical activation at 0.95 V in a 0.1 M SPB solution pH 7 at 25 °C. Digital Diffractograms (DDPs) are shown as insets in both Figures.

nanosheets.

3. Conclusions

In the present work, we have identified the requirements and implications of the potential-induced activation of a **2D-CoMOF@Nafion** composite to boost the oxygen evolution reaction at neutral pH. The results obtained reveal that its electroactivation requires the occurrence of the OER and leads to an increase in the electroactive population of cobalt centers. It has been found that the electroactivation of the MOF can be accelerated upon increasing the applied activation potential in the OER region. The unique linear correlation between the electrocatalytic current and the amount of electroactive cobalt centers, regardless of the activation potential and time, indicates that the catalytic enhancement is due solely to an increase in the number of electroactive cobalt centers, without changing their intrinsic electrocatalytic properties. Structural characterization with advanced techniques revealed that the electrochemical activation produces the dissemination of the Nafion adlayer and morphological changes of the **2D-CoMOF** particles that leads to an increase of the number of surface–exposed cobalt centers accessible to the electrolyte. Interestingly, the electrochemical activation does not alter neither the crystallinity of the MOF at the nanoscale nor the coordinative chemistry of the metal centers. This finding is envisaged to be key for its outstanding electrocatalytic activity for OER at neutral pH. Overall, this work provides a better understanding of the processes, and structural and morphological transformation behind the electrochemical activation of a cobalt MOF for boosting the electrocatalytic water oxidation.

Associated Content

Experimental details, additional electrochemical and microscopy characterization of 2D-CoMOF@Nafion composite are available in the Supporting Information of this article.

Declaration of Competing Interest

The authors declare the following financial interests/personal relationships which may be considered as potential competing interests: 'Pascual Ona Burgos reports financial support was provided by Spanish Government. Pascual Ona Burgos reports financial support was provided by Government of Andalusia. Jose Juan Calvino Gamez reports financial support was provided by European Union.'

Data availability

Data will be made available on request.

Acknowledgments

Authors thank the financial support by the Spanish Government (RTI2018-096399-A-I00, PID2020-113006-RB-I00, PID2021-126799NB-I00, TED2021-130191B-C41, TED2021-130191B-C42 and TED2021-130191B-C44 funded by MCIN/AEI/ 10.13039/501100011033) and Junta de Andalucía (P20-01027 and PYC 20 RE 060 UAL). The authors acknowledge funding from the European Union's Horizon 2020 research and innovation program under Grant 823717-ESTEEM3. Electron microscopy studies were performed at the DME-UCA node of the Spanish Unique Infrastructure (ICTS) on Electron Microscopy of Materials ELECMI. The authors thank Dr. A. Raya-Baron for his support on this work.

Appendix A. Supplementary material

Supplementary data to this article can be found online at https://doi.org/10.1016/j.apsusc.2023.157001.

References

[1] T.Y. Ma, S. Dai, M. Jaroniec, S.Z. Qiao, Metal-organic framework derived hybrid Co3O4-carbon porous nanowire arrays as reversible oxygen evolution electrodes, J. Am. Chem. Soc. 136 (2014) 13925–13931, https://doi.org/10.1021/ja5082553.
[2] Y. Jiao, Y. Zheng, M. Jaroniec, S.Z. Qiao, Design of electrocatalysts for oxygen- and hydrogen-involving energy conversion reactions, Chem. Soc. Rev. 44 (2015) 2060–2086, https://doi.org/10.1039/c4cs00470a.
[3] B.Y. Xia, Y. Yan, N. Li, H. Bin Wu, X.W.D. Lou, X. Wang, A metal-organic framework-derived bifunctional oxygen electrocatalyst, Nat. Energy. 1 (2016) 1–8, https://doi.org/10.1038/nenergy.2015.6.
[4] C.P.B.R.D.L. Smith, M.S. Prévot, R.D. Fagan, Z. Zhang, P.A. Sedach, M.K.J. Siu, S. Trudel, Photochemical route for accessing amorphous metal -oxide materials for water oxidation catalysis, Science. 340 (2013) 60–63.
[5] Q. Qian, Y. Li, Y. Liu, L. Yu, G. Zhang, Ambient fast synthesis and active sites deciphering of hierarchical foam-like trimetal-organic framework nanostructures as a platform for highly efficient oxygen evolution electrocatalysis, Adv. Mater. 31 (2019) 1–8, https://doi.org/10.1002/adma.201901139.
[6] S. Gutiérrez-Tarriño, J.L. Olloqui-Sariego, J.J. Calvente, M. Palomino, G. Mínguez Espallargas, J.L. Jordá, F. Rey, P. Oña-Burgos, Cobalt metal-organic framework based on two dinuclear secondary building units for electrocatalytic oxygen evolution, ACS Appl. Mater. Interfaces. 11 (2019) 46658–46665, https://doi.org/10.1021/acsami.9b13655.
[7] P.Q. Liao, J.Q. Shen, J.P. Zhang, Metal-organic frameworks for electrocatalysis, Coord. Chem. Rev. 373 (2018) 22–48, https://doi.org/10.1016/j.ccr.2017.09.001.
[8] Y. Gong, Z. Hao, J. Meng, H. Shi, P. Jiang, M. Zhang, J. Lin, Two CoII metal-organic frameworks based on a multicarboxylate ligand as Electrocatalysts for water splitting, ChemPlusChem 79 (2014) 266–277, https://doi.org/10.1002/cplu.201300334.
[9] X. Hou, Z. Han, X. Xu, D. Sarker, J. Zhou, M. Wu, Z. Liu, M. Huang, H. Jiang, Controllable amorphization engineering on bimetallic metal–organic frameworks for ultrafast oxygen evolution reaction, Chem. Eng. J. 418 (2021), 129330, https://doi.org/10.1016/j.cej.2021.129330.
[10] K. Huang, S. Guo, R. Wang, S. Lin, N. Hussain, H. Wei, B. Deng, Y. Long, M. Lei, H. Tang, H. Wu, Two-dimensional MOF/MOF derivative arrays on nickel foam as efficient bifunctional coupled oxygen electrodes, Chin. J. Catal. 41 (2020) 1754–1760, https://doi.org/10.1016/S1872-2067(20)63613-0.
[11] H. Miyasaka, Control of charge transfer in donor/aceptor metal-organic frameworks, Acc. Chem. Res. 46 (2013) 248–257, https://doi.org/10.3390/books978-3-03928-487-0.
[12] P. Huo, T. Chen, J. Le Hou, L. Yu, Q.Y. Zhu, J. Dai, Ligand-to-ligand charge transfer within metal-organic frameworks based on manganese coordination polymers with tetrathiafulvalene-bicarboxylate and bipyridine ligands, Inorg. Chem. 55 (2016) 6496–6503, https://doi.org/10.1021/acs.inorgchem.6b00571.
[13] C.F. Leong, B. Chan, T.B. Faust, D.M. D'Alessandro, Controlling charge separation in a novel donor-acceptor metal-organic framework via redox modulation, Chem. Sci. 5 (2014) 4724–4728, https://doi.org/10.1039/c4sc01551g.
[14] L.E. Darago, M.L. Aubrey, C.J. Yu, M.I. Gonzalez, J.R. Long, Electronic conductivity, ferrimagnetic ordering, and reductive insertion mediated by organic mixed-valence in a ferric semiquinoid metal-organic framework, J. Am. Chem. Soc. 137 (2015) 15703–15711, https://doi.org/10.1021/jacs.5b10385.
[15] R. Murase, C.F. Leong, D.M. D'Alessandro, Mixed valency as a strategy for achieving charge delocalization in semiconducting and conducting framework materials, Inorg. Chem. 56 (2017) 14373–14382, https://doi.org/10.1021/acs.inorgchem.7b02090.
[16] Z. Xue, K. Liu, Q. Liu, Y. Li, M. Li, C.Y. Su, N. Ogiwara, H. Kobayashi, H. Kitagawa, M. Liu, G. Li, Missing-linker metal-organic frameworks for oxygen evolution reaction, Nat. Commun. 10 (2019) 1–8, https://doi.org/10.1038/s41467-019-13051-2.
[17] S. Dissegna, K. Epp, W.R. Heinz, G. Kieslich, R.A. Fischer, Defective metal-organic frameworks, Adv. Mater. 30 (2018) 1–23, https://doi.org/10.1002/adma.201704501.
[18] B. Slater, Z. Wang, S. Jiang, M.R. Hill, B.P. Ladewig, Missing linker defects in a homochiral metal-organic framework: tuning the chiral separation capacity, J. Am. Chem. Soc. 139 (2017) 18322–18327, https://doi.org/10.1021/jacs.7b10112.
[19] S. Yuan, J.S. Qin, L. Zou, Y.P. Chen, X. Wang, Q. Zhang, H.C. Zhou, Thermodynamically guided synthesis of mixed-linker Zr-MOFs with enhanced tunability, J. Am. Chem. Soc. 138 (2016) 6636–6642, https://doi.org/10.1021/jacs.6b03263.
[20] Z. Fang, J.P. Dürholt, M. Kauer, W. Zhang, C. Lochenie, B. Jee, B. Albada, N. Metzler-Nolte, A. Pöppl, B. Weber, M. Muhler, Y. Wang, R. Schmid, R.A. Fischer, Structural complexity in metal-organic frameworks: simultaneous modification of open metal sites and hierarchical porosity by systematic doping with defective linkers, J. Am. Chem. Soc. 136 (2014) 9627–9636, https://doi.org/10.1021/ja503218j.
[21] J.Q. Shen, P.Q. Liao, D.D. Zhou, C.T. He, J.X. Wu, W.X. Zhang, J.P. Zhang, X. M. Chen, Modular and stepwise synthesis of a hybrid metal-organic framework for efficient electrocatalytic oxygen evolution, J. Am. Chem. Soc. 139 (2017) 1778–1781, https://doi.org/10.1021/jacs.6b12353.
[22] J. Song, C. Zhu, B.Z. Xu, S. Fu, M.H. Engelhard, R. Ye, D. Du, S.P. Beckman, Y. Lin, Bimetallic cobalt-based phosphide zeolitic imidazolate framework: CoPx phase-dependent electrical conductivity and hydrogen atom adsorption energy for efficient overall water splitting, Adv. Energy Mater. 7 (2017) 1–9, https://doi.org/10.1002/aenm.201601555.
[23] W. Li, S. Watzele, H.A. El-Sayed, Y. Liang, G. Kieslich, A.S. Bandarenka, K. Rodewald, B. Rieger, R.A. Fischer, Unprecedented high oxygen evolution

activity of electrocatalysts derived from surface-mounted metal-organic frameworks, J. Am. Chem. Soc. 141 (2019) 5926–5933, https://doi.org/10.1021/jacs.9b00549.
[24] L. Tao, C.Y. Lin, S. Dou, S. Feng, D. Chen, D. Liu, J. Huo, Z. Xia, S. Wang, Creating coordinatively unsaturated metal sites in metal-organic-frameworks as efficient electrocatalysts for the oxygen evolution reaction: insights into the active centers, Nano Energy 41 (2017) 417–425, https://doi.org/10.1016/j.nanoen.2017.09.055.
[25] Z. Jiang, L. Ge, L. Zhuang, M. Li, Z. Wang, Z. Zhu, Fine-tuning the coordinatively unsaturated metal sites of metal-organic frameworks by plasma engraving for enhanced electrocatalytic activity, ACS Appl. Mater. Interfaces. 11 (2019) 44300–44307, https://doi.org/10.1021/acsami.9b15794.
[26] X.F. Lu, P.Q. Liao, J.W. Wang, J.X. Wu, X.W. Chen, C.T. He, J.P. Zhang, G.R. Li, X. M. Chen, An alkaline-stable, metal hydroxide mimicking metal-organic framework for efficient electrocatalytic oxygen evolution, J. Am. Chem. Soc. 138 (2016) 8336–8339, https://doi.org/10.1021/jacs.6b03125.
[27] Z. Zou, T. Wang, X. Zhao, W.J. Jiang, H. Pan, D. Gao, C. Xu, Expediting in-situ electrochemical activation of two-dimensional metal-organic frameworks for enhanced OER intrinsic activity by iron incorporation, ACS Catal. 9 (2019) 7356–7364, https://doi.org/10.1021/acscatal.9b00072.
[28] Z. Gao, Z.W. Yu, F.Q. Liu, C. Yang, Y.H. Yuan, Y. Yu, F. Luo, Stable Iron hydroxide Nanosheets@Cobalt-metal–organic–framework heterostructure for efficient electrocatalytic oxygen evolution, ChemSusChem 12 (2019) 4623–4628, https://doi.org/10.1002/cssc.201902118.
[29] W. Zheng, L.Y.S. Lee, Metal-organic frameworks for electrocatalysis: catalyst or precatalyst? ACS Energy Lett. 6 (2021) 2838–2843, https://doi.org/10.1021/acsenergylett.1c01350.
[30] M. Salmanion, M.M. Najafpour, Structural changes of a NiFe-based metal-organic framework during the oxygen-evolution reaction under alkaline conditions, Int. J. Hydrogen Energy. 46 (2021) 19245–19253, https://doi.org/10.1016/j.ijhydene.2021.03.107.
[31] X. Yu, Y. Huo, J. Yang, S. Chang, Y. Ma, W. Huang, Reduced graphene oxide supported Au nanoparticles as an efficient catalyst for aerobic oxidation of benzyl alcohol, Appl. Surf. Sci. 280 (2013) 450–455, https://doi.org/10.1016/J.APSUSC.2013.05.008.
[32] G. Zhang, H. Zhou, C. An, D. Liu, Z. Huang, Y. Huang, Bimetallic palladium-gold nanoparticles synthesized in ionic liquid microemulsion, Colloid Polym. Sci. 290 (2012) 1435–1441, https://doi.org/10.1007/S00396-012-2670-6/FIGURES/8.
[33] G.V. Zhutaeva, V.A. Bogdanovskaya, E.S. Davydova, L.P. Kazanskii, M. R. Tarasevich, Kinetics and mechanism of oxygen electroreduction on Vulcan XC72R carbon black modified by pyrolysis products of cobalt 5,10,15,20-tetrakis (4- methoxyphenyl)porphyrine in a broad pH interval, J. Solid State Electrochem. 18 (2014) 1319–1334, https://doi.org/10.1007/S10008-013-2233-X/FIGURES/15.
[34] S. Zuo, Z.P. Wu, H. Zhang, X.W. Lou, Operando monitoring and deciphering the structural evolution in oxygen evolution electrocatalysis, Adv. Energy Mater. 12 (2022), https://doi.org/10.1002/aenm.202103383.
[35] G. Li, L. Lu, L. Pei, Z. Ma, Y. Yuan, M.L. Hu, Q. Miao, J. Zhong, In situ transformation of metal-organic frameworks into hollow nickel-cobalt double hydroxide arrays for efficient water oxidation, Inorg. Chem. 61 (2022) 738–745, https://doi.org/10.1021/acs.inorgchem.1c03602.
[36] S. Zhao, C. Tan, C.T. He, P. An, F. Xie, S. Jiang, Y. Zhu, K.H. Wu, B. Zhang, H. Li, J. Zhang, Y. Chen, S. Liu, J. Dong, Z. Tang, Structural transformation of highly active metal–organic framework electrocatalysts during the oxygen evolution reaction, Nat. Energy. 5 (2020) 881–890, https://doi.org/10.1038/s41560-020-00709-1.
[37] M. Lehene, D. Plesa, S. Ionescu-Zinca, S.D. Iancu, N. Leopold, S.V. Makarov, A.M. V. Brânzanic, R. Silaghi-Dumitrescu, Adduct of aquacobalamin with hydrogen peroxide, Inorg. Chem. 60 (2021) 12681–12684, https://doi.org/10.1021/acs.inorgchem.1c01483.
[38] S. Li, X. Liu, H. Chai, Y. Huang, Recent advances in the construction and analytical applications of metal-organic frameworks-based nanozymes, TrAC - Trends Anal. Chem. 105 (2018) 391–403, https://doi.org/10.1016/j.trac.2018.06.001.
[39] X. Niu, X. Li, Z. Lyu, J. Pan, S. Ding, X. Ruan, W. Zhu, D. Du, Y. Lin, Metal-organic framework based nanozymes: promising materials for biochemical analysis, Chem. Commun. 56 (2020) 11338–11353, https://doi.org/10.1039/d0cc04890a.
[40] L. Ma, F. Jiang, X. Fan, L. Wang, C. He, M. Zhou, S. Li, H. Luo, C. Cheng, L. Qiu, Metal–organic-framework-engineered enzyme-mimetic catalysts, Adv. Mater. 32 (2020), https://doi.org/10.1002/adma.202003065.
[41] M. Li, J. Chen, W. Wu, Y. Fang, S. Dong, Oxidase-like MOF-818 nanozyme with high specificity for catalysis of catechol oxidation, J. Am. Chem. Soc. 142 (2020) 15569–15574, https://doi.org/10.1021/jacs.0c07273.
[42] W. Gao, W. Gou, R. Wei, X. Bu, Y. Ma, J.C. Ho, In situ electrochemical conversion of cobalt Oxide@MOF-74 core-shell structure as an efficient and robust electrocatalyst for water oxidation, Appl. Mater. Today. 21 (2020), 100820, https://doi.org/10.1016/j.apmt.2020.100820.
[43] S. Gutiérrez-Tarriño, J.L. Olloqui-Sariego, J.J. Calvente, G.M. Espallargas, F. Rey, A. Corma, P. Oña-Burgos, Cobalt metal-organic framework based on layered double nanosheets for enhanced electrocatalytic water oxidation in neutral media, J. Am. Chem. Soc. 142 (2020) 19198–19208, https://doi.org/10.1021/jacs.0c08882.
[44] M.C. Biesinger, B.P. Payne, A.P. Grosvenor, L.W.M. Lau, A.R. Gerson, R.S.C. Smart, Resolving surface chemical states in XPS analysis of first row transition metals, oxides and hydroxides: Cr, Mn, Fe, Co and Ni, Appl. Surf. Sci. 257 (2011) 2717–2730, https://doi.org/10.1016/j.apsusc.2010.10.051.
[45] T. Ivanova, A. Naumkin, A. Sidorov, I. Eremenko, M. Kiskin, X-ray photoelectron spectra and electron structure of polynuclear cobalt complexes, J. Electron Spectros. Relat. Phenomena. 156–158 (2007) 200–203, https://doi.org/10.1016/j.elspec.2006.12.005.
[46] J.C. Carver, G.K. Schweitzer, T.A. Carlson, Use of X-ray photoelectron spectroscopy to study bonding in Cr, Mn, Fe, and Co compounds, J. Chem. Phys. 57 (1972) 973–982, https://doi.org/10.1063/1.1678348.
[47] I.S.D.C. Frost, C.A. McDowell, Woolsey, X-ray photoelectron spectra of cobalt compounds, Mol. Phys. 27 (1974) 1473–1489.
[48] D. Briggs, V.A. Gibson, Direct observation of multiplet splitting In 2p photoelectron peaks of cobalt complexes, Chem. Phys. Lett. 25 (1974) 493–496.
[49] Y. Okamoto, H. Nakano, T. Imanaka, S. Teranishi, X-ray photoelectron spectroscopic studies of catalysts — supported cobalt catalysts —, Bull. Chem. Soc. Jpn. 48 (1975) 1163–1168, https://doi.org/10.1246/bcsj.48.1163.
[50] X. Zhang, N. Qu, S. Yang, D. Lei, A. Liu, Q. Zhou, Cobalt induced growth of hollow MOF spheres for high performance supercapacitors, Mater. Chem. Front. 5 (2021) 482–491, https://doi.org/10.1039/d0qm00597e.
[51] J. Cañón, A.V. Teplyakov, XPS characterization of cobalt impregnated SiO2 and γ-Al2O3, Surf. Interface Anal. 53 (2021) 475–481, https://doi.org/10.1002/sia.6935.
[52] X. Hou, J. Wang, B. Mousavi, N. Klomkliang, S. Chaemchuen, Strategies for induced defects in metal-organic frameworks for enhancing adsorption and catalytic performance, Dalt. Trans. 51 (2022) 8133–8159, https://doi.org/10.1039/d2dt01030e.